Journal of Power Sources 195 (2010) 2774–2781

Contents lists available at ScienceDirect

Journal of Power Sources

journal homepage: www.elsevier.com/locate/jpowsour

Mechanical properties of 10 mol% Sc_2O_3–1 mol% CeO_2–89 mol% ZrO_2 ceramics

Nina Orlovskaya[a,*], Svetlana Lukich[a], Ghatu Subhash[b], Thomas Graule[c], Jakob Kuebler[c]

[a] University of Central Florida, Department of Mechanical, Materials and Aerospace Engineering, 4000 Central Florida Boulevard, Orlando, FL 32816-2993, USA
[b] University of Florida, Department of Mechanical and Aerospace Engineering, Gainesville, FL 32611-6250, USA
[c] EMPA, Swiss Federal Laboratories for Materials Testing and Research, Laboratory for High Performance Ceramics, Ueberlandstr. 129, 8600 Duebendorf, Switzerland

ARTICLE INFO

Article history:
Received 26 September 2009
Received in revised form 31 October 2009
Accepted 2 November 2009
Available online 10 November 2009

Keywords:
Young's modulus
Cubic and rhombohedral phase
Zirconia
Strength
Fracture toughness
Stress–strain deformation behavior in compression

ABSTRACT

The mechanical properties, such as Young's modulus, Vickers hardness, indentation fracture resistance, room and high temperature four-point bending strength and SEVNB fracture toughness along with the stress–strain deformation behavior in compression, of 10 mol% Sc_2O_3–1 mol% CeO_2–ZrO_2 ($ScCeZrO_2$) ceramics have been studied. The chosen composition of the $ScCeZrO_2$ has very high ionic conductivity and, therefore, is very promising oxygen ion conducting electrolyte for the intermediate temperature solid oxide fuel cells. Therefore, its mechanical behavior is of importance and is presented in the paper.

1. Introduction

Zirconia based ceramics have attracted increased attention over the last couple of decades for their use in efficient energy systems such as solid oxide fuel cells (SOFCs) and oxygen separation membranes [1,2]. Materials for use in such systems have been characterized extensively with respect to their electrochemical and thermal properties, which are vital in determining how successful the materials could be for a given application. However, when the material has been identified with a superior set of electrochemical and thermal properties its mechanical properties must be characterized to ensure that the new material would be able to withstand the existing loading conditions during operation, and this paper will address the mechanical behavior of promising $Sc_{0.1}Ce_{0.01}ZrO_2$ electrolyte.

Sc_2O_3 doped ZrO_2 ($ScZrO_2$) ceramics have recently attracted a significant interest as a novel electrolyte material for lower temperature SOFCs due to their excellent ionic conductivity [3–5]. There have been numerous reports on the ionic conductivity of $ScZrO_2$ ceramics [6,7] which was reported to be near twice as high as other ZrO_2 based electrolytes [8]. The drawback of $ScZrO_2$ has been also reported as an ordering of vacancies over time, called the aging phenomenon, accompanied by a phase transition to a lower symmetry rhombohedral phase, resulting in decreased conductivity [9]. Most of the studies of $ScZrO_2$ ceramics were performed on the materials with 8–12 mol% doping level of Sc_2O_3, where a cubic phase is a main single phase at 700–800 °C operating temperatures. The highly conductive cubic phase is not stable below 650 °C causing the abrupt decrease in ionic conductivity during cooling in the $ScZrO_2$ [10,11]. It is known that in 11 mol% Sc_2O_3–89 mol% ZrO_2, a cubic to rhombohedral phase transition occurs when the temperature decreases below 600 °C [12,13]. The attempts were made to further stabilize the cubic phase, suppress or fully eliminate cubic to rhombohedral phase transition and prevent the aging phenomenon by substituting 1 mol% of Sc_2O_3 by other oxides such as Yb_2O_3 [13], Bi_2O_3 [14], or Mn_2O_3 [15] among others. It was reported [16,17] that when ZrO_2 is stabilized with a small amount of CeO_2 along with Sc_2O_3, it no longer exhibits an unfavorable phase transition, making this material a very promising option for intermediate temperature electrolytes.

In Ref. [17], the commercially available 10 mol% Sc_2O_3–1 mol% CeO_2–ZrO_2 ($Sc_{0.1}Ce_{0.01}ZrO_2$) manufactured by Daiichi Kigenso Kagaku Kogyo (DKKK, Japan) has been reported to have a stable cubic phase, superior electrical properties and excellent high temperature long term operating characteristics of single cells using $Sc_{0.1}Ce_{0.01}ZrO_2$ as an electrolyte material. Contrary, the reversible and slow cubic to rhombohedral and rhombohedral to cubic phase transitions at 300–500 °C has been reported upon heating of $Sc_{0.1}Ce_{0.01}ZrO_2$ ceramics [18,19], which were probably overlooked in other studies due to slow kinetics of cubic to rhombohedral phase

* Corresponding author. Tel.: +1 4078235770; fax: +1 4078230208.
E-mail address: norlovsk@mail.ucf.edu (N. Orlovskaya).

0378-7753/$ – see front matter © 2009 Elsevier B.V. All rights reserved.
doi:10.1016/j.jpowsour.2009.11.016

transition upon heating. However, it is not expected that these transitions could have a significant effect on $Sc_{0.1}Ce_{0.01}ZrO_2$ electrolyte performance since they occur at lower temperatures and could simply be bypassed during heating up or cooling down cycles of the cells. It was also reported that the kinetics of the phase transition is a strong function of the grain size of the $Sc_{0.1}Ce_{0.01}ZrO_2$ ceramics [18], therefore the transition could be avoided if the grain size of $Sc_{0.1}Ce_{0.01}ZrO_2$ ceramics falls below a certain critical limit. It was also found that the coefficient of thermal expansion of cubic $Sc_{0.1}Ce_{0.01}ZrO_2$ is very close to the Y_2O_3 stabilized ZrO_2 (YSZ) which is a good indicator that $Sc_{0.1}Ce_{0.01}ZrO_2$ ceramics is a perfect candidate for substitution of YSZ electrolyte for IT SOFCs.

To the best of our knowledge there were no reports on mechanical performance of $Sc_{0.1}Ce_{0.01}ZrO_2$ ceramics and this paper aims on filling the gap. There are, however, many similar materials that have been tested to determine their mechanical behavior. Hirano et al. [20] report that increasing scandia doping from 3 to 7 mol% in tetragonal zirconia leads to dramatic decrease in both strength and fracture toughness of the material. For composition with 3 mol% Sc_2O_3 doping strength and fracture toughness were reported to be 640 MPa and 3.8 MPa $m^{1/2}$, respectively, but for 7 mol% Sc_2O_3 doping the properties decreased to 335 MPa and 2.7 MPa $m^{1/2}$ for strength and fracture toughness, respectively. Another paper [21] reports the similar trend for YSZ ceramics, where fracture toughness values of 4.6, 1.3 and 1.8 MPa $m^{1/2}$ were measured for 3, 8 and 11 mol% of Y_2O_3 doping, respectively. The decrease in strength and fracture toughness as a function of doping level is a result of decrease in the amount of metastable phases, such as tetragonal, that contributes to the strengthening by the stress induced tetragonal-to-monoclinic phase transformation. It is also obvious, that the lower crystal symmetry of ZrO_2 phases, such as rhombohedral or tetragonal, have a significant number of defects, such as twins, antiphase domains, dislocations or stacking faults that contribute to toughening by interacting with a moving crack or stress fields, thus absorbing extra energy and providing the material with a higher crack resistance. At the same time, the cubic ZrO_2 phase does not possess any twins, stacking faults, or other significant defects except for the high oxygen vacancies concentration and, therefore, its mechanical properties are expected to be lower than that of the materials with tetragonal or rhombohedral structures.

In this paper the mechanical properties, such as hardness, fracture toughness, and strength at room and high temperatures along with RT compressive stress–strain deformation behavior are reported for cubic and rhombohedral $Sc_{0.1}Ce_{0.01}ZrO_2$ ceramics produced using DKKK powders. The Weibull statistics have been used to characterize the strength distribution of $Sc_{0.1}Ce_{0.01}ZrO_2$ ceramics at room temperature as well as 400 and 1000 °C. For comparison, another $Sc_{0.1}Ce_{0.01}ZrO_2$ material, sintered from powders produced by Praxair, has also been characterized.

2. Experimental procedure

The starting materials were commercially available powders with the nominal composition of 10 mol% Sc_2O_3–1 mol% CeO_2–89 mol% ZrO_2 ($Sc_{0.1}Ce_{0.01}ZrO_2$). One powder was manufactured by Daiichi Kigenso Kagaku Kogyo (DKKK, Japan) using co-precipitation and the other by Praxair Surface Technologies (Praxair, USA) using spray pyrolysis. The selected characteristics, such as sintering behavior, phase stability, and vibrational properties of the materials have been published in Refs. [18,19,22,23].

For the indentation study, the uniaxially pressed at 20 MPa pellets of these powders were sintered at 1100–1600 °C for 2 h with heating/cooling rate of 10 °C min^{-1}. Sintered pellets were first ground using SiC paper and further polished down to 0.1 μm diamond grit size. Hardness tests were performed using a Vickers hardness tester TOKON-2100B in accordance with E 384-84 ASTM standard. Hardness and indentation fracture resistance of samples sintered at 1100–1600 °C were measured using 9.8 N load, but samples sintered at 1500 °C for 2 h (DKKK) and 1600 °C for 2 h (Praxair) were subjected to loads of 0.25, 0.5, 0.98, 2.94, 4.9, 9.8, 29.4, 49.0 and 98.0 N for a period of 15 s. The Vickers hardness H was calculated according to the following formula [24]:

$$H = 0.018187\frac{P}{d^2}\ \text{(GPa)}$$

where P is the load in N, and d is the arithmetic mean of the two diagonals in m.

The indentation fracture resistance K_R was calculated from the resulting Vickers impression by using the following formula [25]:

$$K_R = 0.022\left(\frac{E}{H}\right)^{1/2} \times \left(\frac{P}{c}\right)^{3/2}\ (\text{MPa m}^{1/2})$$

where P is the applied load in N, E is the Young's modulus in GPa, H is the Vickers hardness in GPa, c is the radial crack length measured from the center of the indent in meters, and 0.022 is empirically determined "calibration" constant in ambient air [26,27]. The Young's modulus values used to calculate K_R were obtained from natural frequency measurements at room temperature [28].

5 mm × 6 mm × 45 mm bars were sintered for the measurements of Young's modulus, strength and fracture toughness of $Sc_{0.1}Ce_{0.01}ZrO_2$. First commercially received powders were uniaxially pressed in a steel die at 20 MPa. The samples were subsequently cold isostatically pressed (CIPed) at a pressure of 200 MPa. The bars after uniaxial and cold isostatic pressing were sintered at 1500 °C for DKKK and 1600 °C for Praxair ceramics. The dwell time during sintering was 2 h and 10 °C min^{-1} heating/cooling rate was used. The samples were sintered in air. The machining of the chamfered samples to the final 3 mm × 4 mm × 45 mm dimension was performed in accordance with the EN 843-1 standard.

Young's modulus of the material was measured using the natural frequency method using Gindosonic's mk5 machine (Belgium) in accordance with EN 843-2 standard. The sample with a known density was placed over the microphone lining up with the supporting cylinders. The sample was then struck with a small hammer and the mk5 machine recorded the resulting frequency. The test set and procedure for the Young's modulus measurements at elevated temperatures were modified. Firstly, the specimens were fixed with very fine platinum wires in a small oven. Then, a thin ceramic pipe was lined up with the sample and connected outside the oven to the microphone. A 2nd ceramic pipe was placed above the sample with one end outside the oven. Secondly, the sample was heated up with a rate of 15 °C min^{-1} in air and after reaching a specific temperature the sample was equilibrated for about 10 min. Finally, the natural frequency of the sample was activated by once hitting it with a small ceramic ball using the 2nd pipe as drop guide. For the measurements during cool down the natural cool down rate of the small oven was used.

Flexural strength was measured with the four-point test method in accordance with EN 843-1 standard. Measurements were performed at 25, 400, 600, 800 and 1000 °C. Ten samples were used at each temperature for each composition. Before measurements, the samples were dwelled for 30 min at a given temperature in order for them to come to the thermal equilibrium. They were then preloaded by applying a 10 MPa stress and allowed to rest for an additional 2 min. The crosshead speed was set to 1.5 mm min^{-1} for all samples. Weibull analysis of the strength data was performed in accordance with ENV 843-5 standard and Ref. [29].

Fracture toughness was measured using Single Edge V Notch Beam (SEVNB) technique in accordance with CEN/TS 14425-5 standard. A single notch was made on the 3 mm side of the 3 mm × 4 mm × 45 mm bar as near to the center as possible with

a depth between 20 and 40% of the total depth of the bar, since it was shown that within this range the depth of the notch has no influence on the K_{Ic} values [30]. A notch making machine was used to ensure the greatest amount of consistency between notches. The machine drove a razor blade to oscillate back and forth across the specimen. The tip of the blade was coated with a diamond paste that varied from a particle size of 10 μm for the course notch to 1 μm for sharpening the notch. The tip radius was monitored so that no specimen had a tip radius larger than 5 μm in accordance with CEN/TS 14425-5 standard. Fracture toughness tests were performed at 25, 200, 400, 600, 800 and 1000 °C. Three specimens were used at each temperature for each composition. Samples were given a minimum of 30 min to come to thermal equilibrium. They were then preloaded by applying a 10 N force and allowed to rest for additional 2 min. The crosshead speed was set to 0.1 mm min^{-1} for all samples.

Compression tests were performed in a servo-hydraulic test machine (Instron 8500) with a 20 kN load cell. The $Sc_{0.1}Ce_{0.01}ZrO_2$ samples for compression experiments were machined into cylinders 6 mm in diameter and 12 mm in height. The compression load was applied along the sample's maximum dimension and the strain was measured using three strain gauges placed on the lateral faces of the specimen, along the loading direction. The samples were loaded to 700 MPa followed by complete unloading at constant loading/unloading rate of 3 MPa s^{-1}. The strain was calculated as an average value given by their different strain gauges signals.

Scanning electron microscopy (Zeiss-SEM) was used for the analysis of fracture surfaces of the $Sc_{0.1}Ce_{0.01}ZrO_2$ bars after mechanical tests.

3. Results and discussion

3.1. Stability, lattice parameters, and densities of the cubic and rhombohedral $Sc_{0.1}Ce_{0.01}ZrO_2$

The cubic phase is a metastable phase in $Sc_{0.1}Ce_{0.01}ZrO_2$ at room temperature [18] owing its existence to the relatively fast cooling of the ceramic from the sintering temperature. It should be noted that at 700–800 °C, which are SOFC operating temperatures, the cubic phase is stable and will not transform to any other phase degrading SOFC performance. However for the applications at lower temperature, especially in around 400 °C region, the cubic phase will eventually transform to the thermodynamically more stable rhombohedral phase [31,12]. The measured lattice parameter a is almost identical for DKKK and Praxair materials and is equal to 5.09119(7) and 5.09203(7) Å, respectively [18]. Using these lattice parameters, the theoretical density of DKKK and Praxair ceramics equals to 5.827 and 5.845 g cm^{-3}, respectively. In order to fully convert cubic $Sc_{0.1}Ce_{0.01}ZrO_2$ to the rhombohedral phase, as sintered cubic $Sc_{0.1}Ce_{0.01}ZrO_2$ ceramics were annealed at 400 °C for 12 h. After the heat treatment, only rhombohedral phase has been detected at room temperature with about 3% of c phase and a very small amount of $8ZrO_2{\cdot}2Sc_2O_3$ are still present [18]. The calculated lattice parameter of β-phase is $a = 3.56596(3)$ Å and $c = 9.00992(1)$ Å, space group $R\bar{3}$ (#148). Theoretical density of β-phase calculated from lattice parameters is 5.721 g cm^{-3} and is slightly lower than that of the cubic phase.

3.2. Young's modulus of cubic and rhombohedral $Sc_{0.1}Ce_{0.01}ZrO_2$

The room temperature Young's modulus, measured by the ultrasonic technique was found to be equal to 217.67 ± 0.61 and 188.23 ± 2.81 GPa for cubic DKKK ceramics sintered at 1500 °C and Praxair ceramics sintered at 1600 °C, respectively. Young's modulus of cubic yttria stabilized ZrO_2 was reported to be 220 GPa [33], which lines up almost identically with E values of DKKK $Sc_{0.1}Ce_{0.01}ZrO_2$. The lower Young's modulus of Praxair ceramics can be explained by higher porosity of this ceramic. The Young's modulus of annealed rhombohedral $Sc_{0.1}Ce_{0.01}ZrO_2$ was measured to be 211.07 ± 3.28 GPa at RT. The measured Young's modulus values were used for calculation of the indentation fracture resistance of the DKKK and Praxair ceramics.

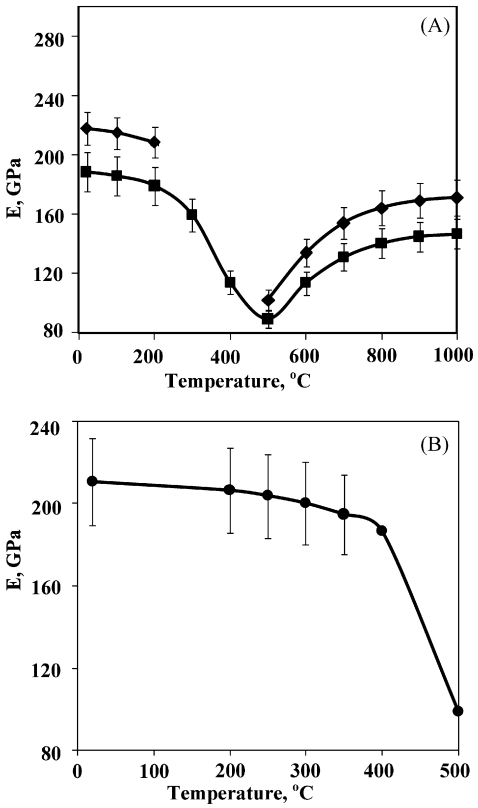

Fig. 1. Young's modulus vs. temperature of (A) the cubic phase sintered from Praxair (–■–) and DKKK (–♦–) powders, and (B) the rhombohedral DKKK (–●–) $Sc_{0.1}Ce_{0.01}ZrO_2$ ceramics.

The Young's modulus of cubic Sc_2O_3–CeO_2–ZrO_2 DKKK ceramics exhibits insignificant softening as temperature increase from room temperature to 200 °C (Fig. 1A). Sc_2O_3–CeO_2–ZrO_2 exhibit a significant mechanical damping in the 300–450 °C temperature range with a simultaneous decrease in Young's modulus values [34]. Because of the high damping the measurements of Young's modulus at 300 and 400 °C were not possible to perform by the impulse excitation technique. A significant softening of the cubic phase has occurred at 500 °C and Young's modulus values decrease to 102.07 ± 0.47 GPa at this temperature. As temperature increased further, Young's modulus of $ScCeZrO_2$ increased from 102.07 ± 0.47 GPa at 500 °C to 171.01 ± 0.79 GPa at 1000 °C. Similar trend was observed for the elastic behavior cubic $ScCeZrO_2$ produced using Praxair powders (Fig. 1A). A non-significant softening from 211.07 ± 3.28 GPa at room temperature to 186.95 ± 0.82 GPa at 400 °C had been observed for the rhombohedral $ScCeZrO_2$ (Fig. 1B). Since the rhombohedral phase is stable up to 400 °C, and upon further increase in temperature will transform to the cubic phase [32], the measurements performed at 500 °C show the property of the cubic $ScCeZrO_2$. The Young's modulus of the rhombohedral phase at 500 °C has a value of 99 GPa which is almost twice as low as the Young's modulus of rhombohedral phase at 400 °C, but corresponded well for the elastic modulus of the cubic phase at 500 °C (Fig. 1A).

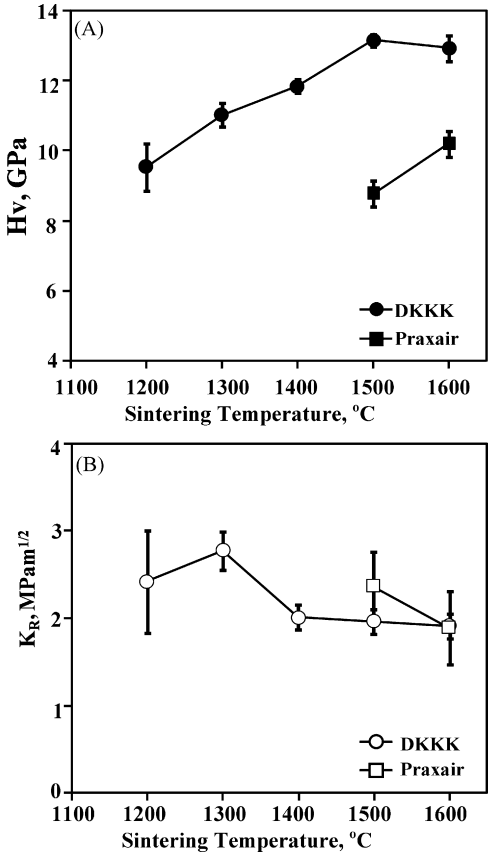

Fig. 2. Hardness (A) and indentation fracture resistance (B) vs. sintering temperature for DKKK and Praxair $Sc_{0.1}Ce_{0.01}ZrO_2$ ceramics.

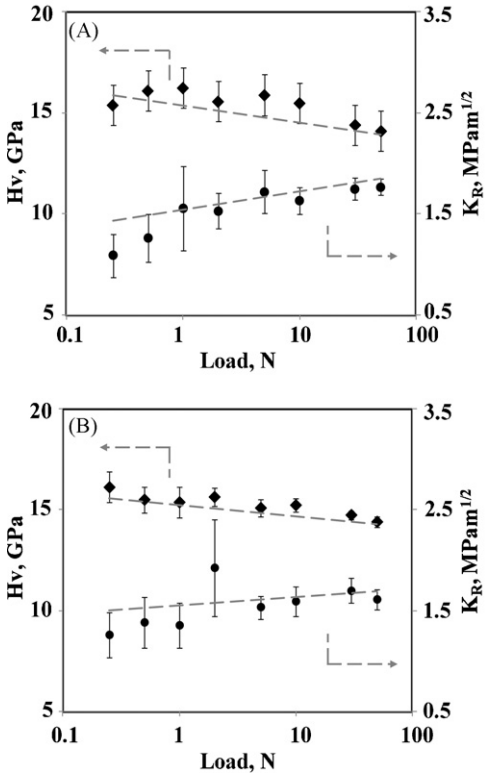

Fig. 3. Hardness (–♦–) and indentation fracture resistance (–●–) of cubic (A) and rhombohedral (B) DKKK $Sc_{0.1}Ce_{0.01}ZrO_2$.

3.3. Hardness and indentation fracture resistance

The Vickers hardness and fracture resistance of $Sc_{0.1}Ce_{0.01}ZrO_2$ ceramics sintered at different temperatures are shown in Fig. 2. Density and grain size of the $Sc_{0.1}Ce_{0.01}ZrO_2$ ceramics increase with increase of the sintering temperature [18], and the hardness of the ceramics increases too (Fig. 2A). There is almost linear increase of hardness of DKKK ceramics from 9.53 ± 0.67 GPa sintered at 1200 °C to 13.14 ± 0.18 GPa sintered at 1500 °C. This could be well explained by the significant increase of the density of the sintered ceramics [32]. The hardness of DKKK ceramics remains the same for the material sintered at 1500 and 1600 °C. The hardness of DKKK ceramics was found to be higher than the hardness of $Sc_{0.1}Ce_{0.01}ZrO_2$ ceramics made from Praxair powder. This could be explained that the Praxair ceramics contain a significant amount of porosity (7.1 and 4.4%) even when sintered at 1500 and 1600 °C, respectively. The porosity has a detrimental effect on hardness, and even a small amount of residual porosity could significantly decrease hardness. Therefore, such difference in hardness as 13.14 ± 0.18 and 8.76 ± 0.36 GPa for DKKK and Praxair $Sc_{0.1}Ce_{0.01}ZrO_2$ ceramics could be explained by the significant difference in their porosity after sintering at 1500 °C.

The porosity plays a role by increasing the material's resistance to crack propagation. Thus, the measured K_R values of cubic DKKK ceramics sintered at 1600 °C is equal to 1.91 ± 0.14 MPa $m^{1/2}$, however K_R becomes equal to 2.42 ± 0.58 MPa $m^{1/2}$ for ceramics sintered at 1200 °C with a high level of porosity 13.6%. The ceramics made from Praxair powder have similar K_R values as DKKK $Sc_{0.1}Ce_{0.01}ZrO_2$.

The hardness and fracture resistance of cubic and rhombohedral $Sc_{0.1}Ce_{0.01}ZrO_2$ DKKK ceramics as a function of indentation load are presented in Fig. 3. While the rhombohedral $Sc_{0.1}Ce_{0.01}ZrO_2$ exhibits indentation size effect, where the hardness values decrease from 16.13 ± 0.76 GPa at 0.25 N load to 14.39 ± 0.25 GPa at a load of 50 N (Fig. 3B), the cubic phase does not show the increase of the hardness at small loads (Fig. 3A). Indentation fracture resistance increases as the load increases. It should be noted, that at small loads, such as 0.25, 0.50, 1.00 N the cracks were originated not from all corners of impression, but about 25% of all corners resulted in crack formation.

3.4. Strength and fracture toughness

The room temperature (RT) strength of cubic DKKK $Sc_{0.1}Ce_{0.01}ZrO_2$ ceramics was measured to be 201.29 ± 39.7 MPa and it decreased to 170.10 ± 10.96 MPa at 1000 °C (Fig. 4A). The typical defect, which served as a fracture origin of the DKKK ceramics tested at RT is shown in Fig. 5. While DKKK ceramics show satisfactory strength in comparison with other ceramics used as electrolyte (Table 1), the strength of $Sc_{0.1}Ce_{0.01}ZrO_2$ made of Praxair powder shows much lower values. Thus, Praxair ceramics have RT strength of 78.54 ± 7.53 MPa, which decreases to 59.53 ± 6.77 MPa at 400 °C and remains in the 50–60 MPa range at higher temperature measurements (Fig. 4A). Such decrease in

Table 1
Room and high temperature strength of perspective electrolyte materials.

Material	RT strength (MPa)	800 °C strength (MPa)
$Sc_{0.1}Ce_{0.01}ZrO_2$, DKKK	201.29 ± 39.7	162.14 ± 11.65
$Sc_{0.1}Ce_{0.01}ZrO_2$, Praxair	78.54 ± 7.53	52.13 ± 10.23
$Gd_{0.1}CeO_2$ [45]	120	169
$Y_{0.08}$ SZ [46]	214	146
$La_{0.8}Sr_{0.2}G_{0.08}Mg_{0.2}O_3$ [47]	121	126
$Sc_{0.03}ZrO_2$ [48]	640	
$Sc_{0.07}ZrO_2$ [48]	330	

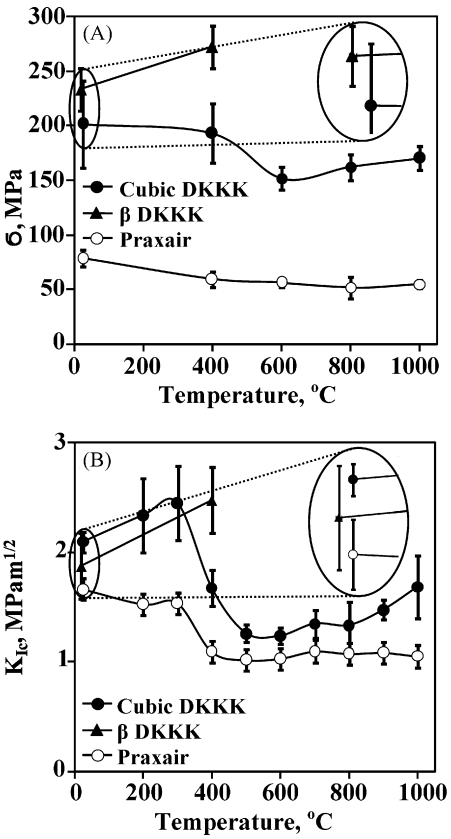

Fig. 4. High temperature four-point bending strength (A) and SEVNB fracture toughness (B) of cubic and rhombohedral DKKK along with cubic Praxair $Sc_{0.1}Ce_{0.01}ZrO_2$ ceramics.

strength in comparison with DKKK ceramics could be explained by the presence of very inhomogeneous areas in sintered Praxair ceramics, with some of the areas being very porous and other being more dense. At the same time the significant amount of the exaggerated grains could be also detected giving a bimodal grain size distribution and definitely affecting the strength of $Sc_{0.1}Ce_{0.01}ZrO_2$ Praxair ceramics (Fig. 6).

The fracture toughness of two ceramics as a function of temperature is shown in Fig. 4B. The room temperature K_{Ic} of DKKK $Sc_{0.1}Ce_{0.01}ZrO_2$ ceramics is equal to 2.09 ± 0.09 MPa m$^{1/2}$ and it increases at 300 °C to 2.44 ± 0.33 MPa m$^{1/2}$, followed by a decrease to 1.26 ± 0.08 MPa m$^{1/2}$ at 500 °C. The further slight increase to 1.68 ± 0.29 MPa m$^{1/2}$ occurs as the temperature increases to

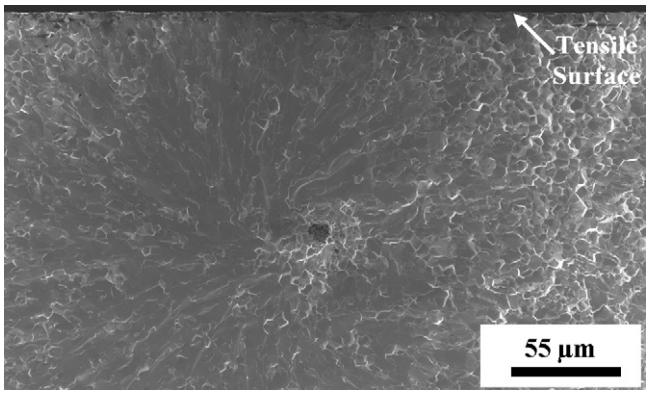

Fig. 5. A pore as a fracture origin of DKKK $Sc_{0.1}Ce_{0.01}ZrO_2$ ceramics tested at RT and 800 °C.

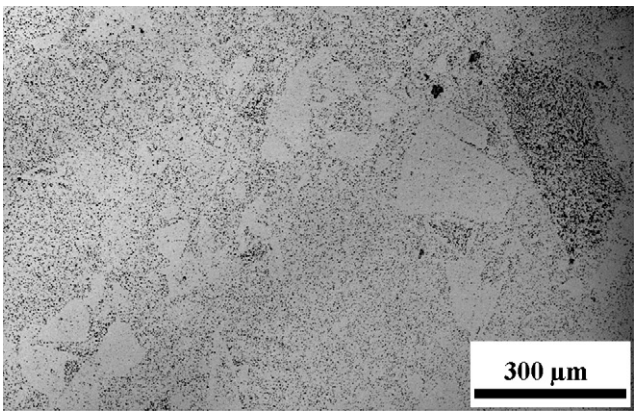

Fig. 6. The polished surface of Praxair $Sc_{0.1}Ce_{0.01}ZrO_2$ ceramics sintered at 1600 °C showing the presence of the non-homogeneous microstructure and porosity.

1000 °C. The increase of the fracture toughness temperature range could be explained by ordering/clustering of oxygen vacancies around the Sc^{3+} dopant cations which were reported to happen at ~300 °C. This ordering/clustering process causes the appearance of the loss peak, the appearance of which shows that there is energy absorbing process occurring at these temperatures [35–37]. Since the cubic to rhombohedral phase transition occurs at 300–400 °C during long annealing time up to 12 h at these temperatures, the reported vacancies ordering phenomenon might be a beginning of the phase transition in $Sc_{0.1}Ce_{0.01}ZrO_2$. The decrease of K_{Ic} at 500 °C can be explained by a significant softening of the lattice and decrease of Young's modulus at this temperature. The second slight increase in K_{Ic} at 900–1000 °C can be explained by the deviation of the oxygen content from its stoichiometric values because oxygen is leaving the crystal lattice creating more vacancies. Such increase of non-stoichiometry leads to the formation of the repulsive forces between cations in the lattice, which, in turn can contribute to the increase in K_{Ic} (Fig. 4B). The fracture toughness of $Sc_{0.1}Ce_{0.01}ZrO_2$ Praxair ceramics was measured to be lower than K_{Ic} of ceramics made of DKKK powders, partly due to lower Young's modulus of this ceramics. Small decrease in K_{Ic} of Praxair ceramics from 1.52 ± 0.01 MPa m$^{1/2}$ at 200 and 300 °C to ~1 MPa m$^{1/2}$ at 400 °C and higher temperatures is reported. The decrease happens in the same temperature range as in the case of DKKK ceramics.

The strength of rhombohedral $Sc_{0.1}Ce_{0.01}ZrO_2$ was slightly higher than those of cubic phase at room temperature and it increased from 233.08 ± 32.01 MPa at RT to 271.80 ± 91.96 MPa when tested at 400 °C (Fig. 4A). One would expect that fracture toughness of rhombohedral phase would be also higher than those of cubic phase, but in fact K_{Ic} of rhombohedral phase was lower than cubic phase at RT, and it increased from 1.87 ± 0.05 MPa m$^{1/2}$ at room temperature to 2.47 ± 0.17 MPa m$^{1/2}$ at 400 °C (Fig. 4B). Such low values of fracture toughness of rhombohedral $Sc_{0.1}Ce_{0.01}ZrO_2$ are indicative that no significant toughening mechanism is active during the deformation of this material despite its rather highly defective microstructure [18].

The fracture surfaces of DKKK ceramics after K_{Ic} tests at RT and 1000 °C are shown in Fig. 7. While fracture surface shows fully transgranular mode of failure after testing at RT (Fig. 7A), the high percentage (~50%) of intergranular fracture appears after tests performed at 1000 °C (Fig. 7B). The intergranular fracture also appears for the samples tested at 800 and 900 °C, but percentage of the intergranular fracture decreases as temperature of test decreases. The intergranular fracture cannot be detected in DKKK ceramics tested at 600 °C or lower temperatures, when only fully transgranular frac-

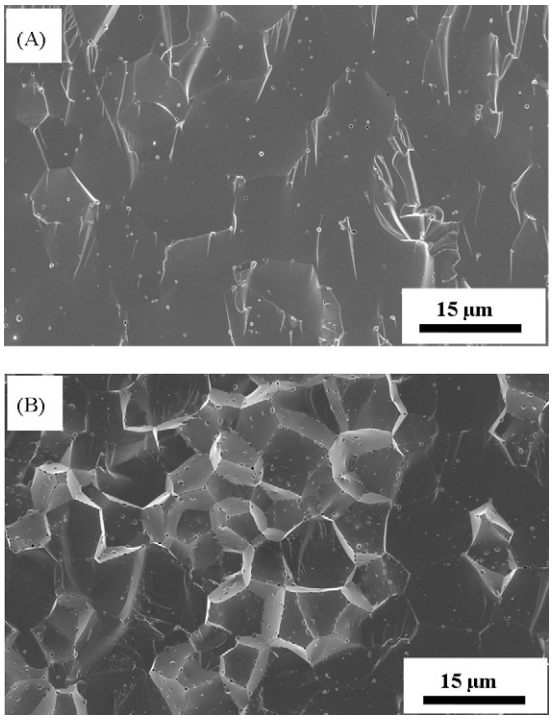

Fig. 7. Fracture surface of DKKK $Sc_{0.1}Ce_{0.01}ZrO_2$ ceramics after K_{Ic} measurement at RT (A) and 1000 °C (B).

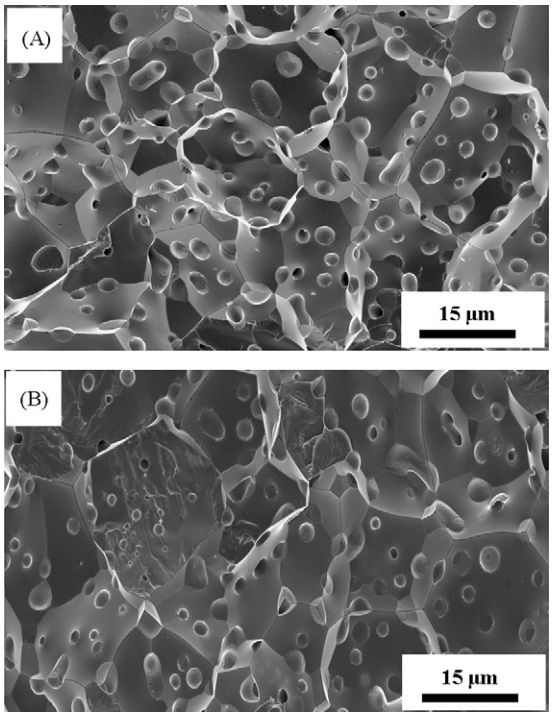

Fig. 8. Fracture surface of Praxair $Sc_{0.1}Ce_{0.01}ZrO_2$ ceramics after K_{Ic} measurement at RT (A) and 1000 °C (B).

ture surfaces are observed. If considered that the vacancies start to appear at 700–800 °C and their amount significantly increases at 900 and 1000 °C, the vacancies will introduce more and more repulsive forces between cations, which in turn put the grains under compressive stresses. These stresses are responsible for the increase of the fracture toughness at higher temperature, but at the same time they force a crack to move not across the grains, but choose easier path along the grain boundaries, causing the appearance of the intergranular failure mode.

The fracture surfaces of $Sc_{0.1}Ce_{0.01}ZrO_2$ Praxair ceramics after K_{Ic} tests performed at RT and 1000 °C are shown in Fig. 8. The porosity with a pore size of about 1.28 μm is present along almost all grain boundaries and inside the grains. The fracture mode is almost fully intergranular. As it was reported in Ref. [18], the Praxair ceramics have higher quantity of SiO_2, which affect the sinterability of the material to the full density. It is also possible that the presence of SiO_2 is responsible for smaller formation of oxygen vacancies when temperature increases, thus there is no increase in fracture toughness at 800–1000 °C region, since $Sc_{0.1}Ce_{0.01}ZrO_2$ Praxair ceramics remain more stoichiometric upon heating.

Fracture origin of the rhombohedral $Sc_{0.1}Ce_{0.01}ZrO_2$ was typical defects, such as pores or cracks, which can be found in ceramics and which are introduced during machining or processing of the samples. An example of a typical fracture origin is shown in Fig. 9A. The fracture surface of rhombohedral phase after strength measurement at RT is shown in Fig. 9B. The relief of the fracture surface of the rhombohedral $Sc_{0.1}Ce_{0.01}ZrO_2$ is much more coarse and complex in comparison with smooth and flat fracture surface of cubic-$Sc_{0.1}Ce_{0.01}ZrO_2$, which indicates that there should be some barriers present for the propagating crack causing it to deviate. Similar fracture surface was observed after tests at 400 °C. The appearance of rough path for the propagating crack might be the reason why strength of the rhombohedral phase is higher than strength of the cubic phase. However, this did not affect the K_{Ic} which remain quite low and was measured to be lower for rhombohedral in comparison with cubic DKKK ceramics (Fig. 4B).

3.5. Weibull analysis of flexural strength

Weibull plots for the DKKK and Praxair $Sc_{0.1}Ce_{0.01}ZrO_2$ tested at RT, 400, and 1000 °C are shown in Fig. 10. To obtain the strength values, 20 bending tests were performed at room temperature, and 9–10 samples were tested at 400 and 1000 °C. The two parameter Weibull distribution is used, with the scale parameter, σ_0, describing the strength, and Weibull modulus, m, which characterize the width of this strength distribution [38–43]. The scale parameter σ_0 and Weibull modulus m calculated from the distributions are presented in Table 2. From Fig. 10 one can see that the material does not perfectly obey Weibull's law and deviations from the straight line, which is the Weibull fit, exist. These deviations significantly affect the Weibull modulus, however the scale parameter is much less affected [30]. More than 10 samples, typically at least 30, have to be tested in order to receive reliable Weibull statistics, but for this research the Weibull parameters were calculated using strength measurements from 9 to 10 samples at higher temperatures, which might contribute to the uncertainty in the estimation of Weibull parameters.

The Weibull modulus m calculated using DKKK and Praxair ceramics falls in the range of 10–18 for most of the tempera-

Table 2
Weibull parameters of DKKK and Praxair ceramics calculated from four-point bending tests performed at different temperatures.

	Temperature	m	σ_0
DKKK ceramics	RT	10.4	217
	400 °C	8	205
	1000 °C	18.1	175
Praxair ceramics	RT	12.5	82
	400 °C	10	63
	1000 °C	17.7	57

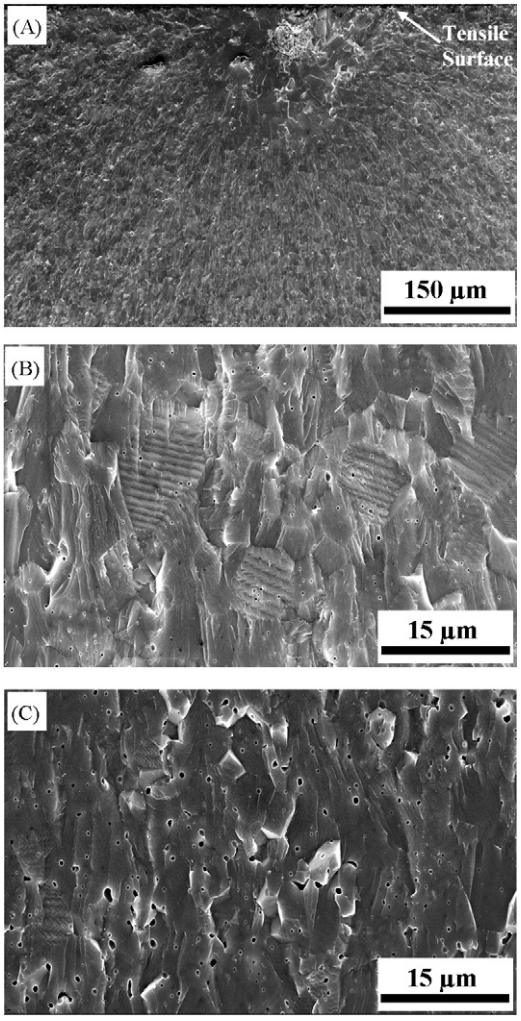

Fig. 9. (A) Fracture origin; (B) fracture surface after RT test; and (C) fracture surface after 400 °C test of the rhombohedral DKKK $Sc_{0.1}Ce_{0.01}ZrO_2$ ceramics.

tures. However, for strength measurements of DKKK ceramics at 400 °C, m is equal to 8 was calculated. The lower m values could be explained by a formation of rhombohedral precipitates in the cubic $Sc_{0.1}Ce_{0.01}ZrO_2$ during the measurements which could serve as additional critical defects to already present pores and other voids inside the ceramic.

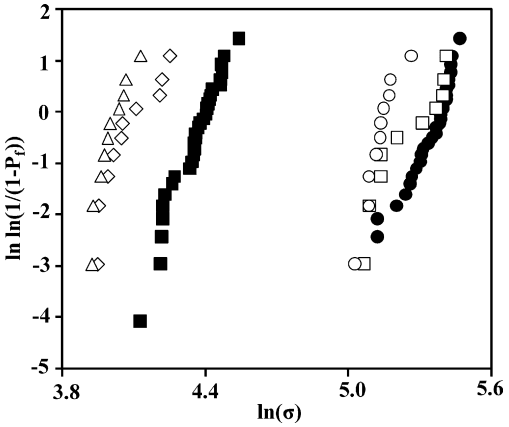

Fig. 10. Weibull plots of the strength distribution of Praxair ((■) RT, (◊) 400 °C, (△)1000 °C) and DKKK ((●) RT, (□) 400 °C, (○) 1000 °C) $Sc_{0.1}Ce_{0.01}ZrO_2$ ceramics.

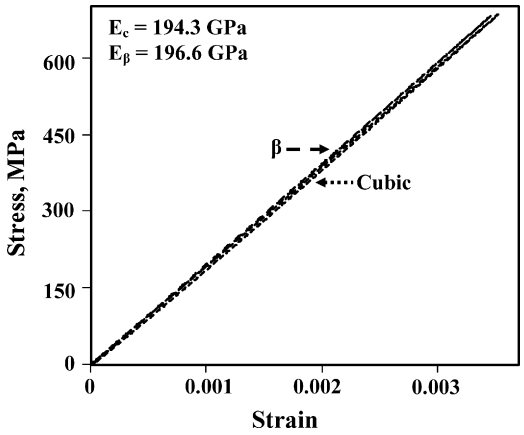

Fig. 11. Stress–strain deformation curves of cubic and rhombohedral DKKK $Sc_{0.1}Ce_{0.01}ZrO_2$ measured in unaxial compression.

3.6. Stress–strain deformation of cubic and rhombohedral $Sc_{0.1}Ce_{0.01}ZrO_2$ in compression

In order to verify the elastic behavior of cubic and rhombohedral $Sc_{0.1}Ce_{0.01}ZrO_2$, the unaxial compression tests were performed (Fig. 11). Through it was expected that nonelastic and possibly ferroelastic behavior could be observed during the deformation of the rhombohedral $Sc_{0.1}Ce_{0.01}ZrO_2$ due to its highly defective microstructure, however both cubic and rhombohedral phases did not show any hysteretic behavior upon loading. The loading and unloading parts at the deformations curves of both cubic and rhombohedral phase have been completely overlapped with no hysteresis observed. These results are in conformity with low K_{Ic} values of the cubic and rhombohedral phases, indicating that defects present inside grains are not mobile at the used stresses and cannot contribute to the toughening of the rhombohedral $Sc_{0.1}Ce_{0.01}ZrO_2$.

The Young's modulus has been calculated from the loading part of the deformation curve. The Young's moduli of both phases are quite similar and are equal to E_{cubic} = 194 GPa and E_β = 196 GPa. The difference between Young's moduli of two ceramics measurement by two techniques could be explained by slight misalignment of the samples during compression, thus giving the lower value of the moduli. It is known that Young's modulus measured by impulse excitation techniques gives the most precise value, but some errors can occur when Young's modulus is measured as a slope of the stress–strain deformation curve [44].

4. Conclusions

The mechanical properties, such as hardness, indentation fracture resistance, Young's modulus, strength, fracture toughness, Weibull parameters, along with stress–strain deformation behavior of $Sc_{0.1}Ce_{0.01}ZrO_2$ have been measured. The ceramics were sintered from the powders produced by two manufactures—DKKK and Praxair. Both DKKK and Praxair ceramics were found to exist in the cubic structure upon cooling of the samples from sintering temperature, however it was found that DKKK cubic phase could be transformed to the rhombohedral phase by dwelling at 375–400 °C for 12 h. Young's moduli of the cubic and rhombohedral phases of DKKK ceramics are reported to be 217.67 ± 0.61 and 188.23 ± 2.81 GPa, respectively. The softening of both cubic DKKK and Praxair and rhombohedral DKKK phases has been observed when the temperature of the tests increased up to 500 °C, but stiffening of the cubic phases occurred when temperature was increased from 500 to 1000 °C. Hardness of the DKKK and Praxair ceramics increased as sintering temperature and density of the materials were increased,

but fracture toughness remains almost the same, with some slight increase for the ceramics sintered at lower temperature which have higher amount of the porosity. No significant indentation size effect has been observed for cubic $Sc_{0.1}Ce_{0.01}ZrO_2$, but non-significant decrease in ~2 GPa in hardness was detected in rhombohedral $Sc_{0.1}Ce_{0.01}ZrO_2$ when the indentation load was increased from 0.25 to 50 N load. Four-point bending strength of the cubic and rhombohedral DKKK ceramics is on the order of 200–230 MPa at room temperature. Strength decreases to 150–170 MPa at higher temperatures for cubic phase, but increases to 270 MPa at 400 °C for the rhombohedral phase. The Praxair $Sc_{0.1}Ce_{0.01}ZrO_2$ exhibits the lower strength values in the range of 80 MPa at room temperature to 60 MPa at high temperatures. Fracture toughness measured in bending using V notched samples was also higher for DKKK $Sc_{0.1}Ce_{0.01}ZrO_2$ ceramics than for Praxair ceramics both at room and high temperatures. The microstructural characterization revealed that Praxair ceramics has very inhomogeneous grain and porosity distribution where selected areas could have a significant amount of porosity while the majority of the grains still have intra- and intergranulated porosity.

DKKK ceramics exhibited intergranular fracture for tests performed at room temperature, but at high temperature the mixed fracture occurs and both intergranular and transgranular fracture modes could be found. The rhombohedral $Sc_{0.1}Ce_{0.01}ZrO_2$ ceramics exhibit the complex relief on the fracture surface with the surface structure that required special detailed studies. The compression of the cubic and rhombohedral phases revealed that both phases behave in the elastic way and no hysteresis is observed upon loading/unloading.

Acknowledgements

This work was supported by the NSF DMR project number 0502765. The authors would also like to thank Mr. R. Bächtold for his help in performing the mechanical tests at EMPA.

References

[1] N.Q. Minh, J. Am. Ceram. Soc. 76 (1993) 563–588.
[2] P. Knauth, H. Tuller, J. Am. Ceram. Soc. 85 (2005) 1654–1680.
[3] I. Kosacki, H.U. Anderson, Y. Mizutani, K. Uaki, Solid State Ionics 152/153 (2002) 431–436.
[4] Z. Lei, Q. Zhu, Solid State Ionics 176 (2005) 2791–2797.
[5] V.V. Kharton, F.M.B. Marques, A. Atkinson, Solid State Ionics 174 (2004) 135–149.
[6] S.P.S. Badwal, S.F. Ciacchi, S. Rajendran, J. Drennan, Solid State Ionics 109 (1998) 167–186.
[7] O. Yamamoto, Y. Arachi, Y. Takeda, N. Imanishi, Y. Mizutani, M. Kawai, Y. Nakamura, Solid State Ionics 79 (1995) 137–142.
[8] Y. Arachi, H. Sakai, O. Yamamoto, Y. Takeda, N. Imanishi, Solid State Ionics 121 (1999) 133–139.
[9] C. Haering, A. Roosen, H. Schichl, M. Schnoller, Solid State Ionics 176 (2005) 261–268.
[10] H. Yamamura, N. Utsunomiya, T. Mori, T. Atake, Solid State Ionics 107 (1998) 185–189.
[11] Y. Arachi, T. Asai, O. Yamamoto, Y. Takeda, N. Imanishi, K. Kawate, C. Tamakoshi, J. Electrochem. Soc. 148 (2001) A520–A523.
[12] M. Yashima, M. Kakihana, M. Yoshimura, Solid State Ionics 86–88 (1996) 1131–1149.
[13] H. Fujimori, M. Yashima, M. Kakihana, M. Yoshimura, J. Appl. Phys. 91 (2002) 6493–6498.
[14] M. Hirano, T. Oda, K. Ukai, Y. Mizutani, J. Am. Ceram. Soc. 85 (2002) 1336–1338.
[15] Z. Lei, Q. Zhu, Mater. Lett. 61 (2007) 1311–1314.
[16] D.S. Lee, W.S. Kim, S.H. Choi, J. Kim, H.W. Lee, J.H. Lee, Solid State Ionics 176 (2005) 33–39.
[17] Z. Wang, M. Cheng, Z. Bi, Y. Dong, H. Zhang, Z. Feng, C. Li, Mater. Lett. 59 (2005) 2579–2582.
[18] S. Yarmolenko, J. Sankar, N. Bernier, M. Klimov, J. Kapat, N. Orlovskaya, J. Fuel Cell Sci. Technol. 6 (2009) 021007 1-8.
[19] A. Zevalkink, A. Hunter, M. Swanson, C. Johnson, J. Kapat, N. Orlovskaya, Mater. Res. Soc. Symp. Proc. (2007) 972–978.
[20] M. Hirano, S. Watanabe, E. Kato, Y. Mizutani, Y. Kawai, Y. Nakamura, Solid State Ionics 111 (1998) 161–169.
[21] Y. Mizutani, M. Tamura, M. Kawai, O. Yamamoto, Solid State Ionics 72 (1994) 271–275.
[22] S. Lukich, C. Carpenter, N. Orlovskaya, J. Power Sources (2009), in press.
[23] S. Lukich, N. Orlovskaya, C. Carpenter, in: D. Singh, J. Salem (Eds.), Proceedings of the 33rd International Conference on Advanced Ceramic and Composites, WILEY, 2009, pp. 4–14.
[24] G.E. Dieter, Mechanical Metallurgy, 3rd ed., Mc-Graw-Hill Bo. Comp., Boston, 1986.
[25] G.R. Anstis, P. Chantikul, B.R. Lawn, D.B. Marshall, J. Am. Ceram. Soc. 64 (1981) 533.
[26] D.J. Morris, R.F. Cook, J. Am. Ceram. Soc. 87 (2004) 1494.
[27] R.F. Cook, Strength characterization of ceramics using controlled indentation flaws, PhD Thesis, University of New South Wales, Sydney, NSW, Australia (1985).
[28] E 1876-99 ASTM "Standard Test Method for Dynamic Young's Modulus, Shear Modulus, and Poisson's Ratio by Impulse Excitation of Vibration".
[29] N. Orlovskaya, H. Peterlik, M. Marczewski, K. Kromp, J. Mater. Sci. 3 (1997) 978–983.
[30] J. Kuebler, Fracture toughness of ceramics using the SEVNB method: first results of a joint VAMAS/ESIS Round Robon. In: E. Ustundag, G. Fischman, Ceramic Engineering and Science Proceedings, Am. Ceram. Soc., 20 (3) (1999) 495–502.
[31] R. Chiba, T. Ishii, F. Yoshimura, Solid State Ionics 91 (1996) 249–256.
[32] M.B. Barsoum, Fundamental of Ceramics, IOP, 2003, p. 188.
[33] M. Taneja, M. Radovic, N. Orlovskaya, Solid State Ionics (submitted for publication).
[34] M. Weller, in: R. Schaller, G. Fantozzi, G. Gremaund (Eds.), Point Defects Relaxations, in a Book "Mechanical Spectroscopy Q^{-1} with Application to Materials Science", Trans Tech Publications, Switzerland, 2001, pp. 95–137.
[35] J.B. Wachtman, Phys. Rev. B 131 (1963) 517–527.
[36] M. Welle, J. Alloy Compd. 211/212 (1994) 66–70.
[37] M. Weller, B. Damson, A. Lakki, J. Alloy Compd. 310 (2000) 47–53.
[38] W. Weibull, J. Appl. Mech. 18 (1951) 293–297.
[39] R. Danzer, J. Eur. Ceram. Soc. 10 (1992) 461–472.
[40] K. Trustrum, A.S. Jayatilaka, J. Mater. Sci. 14 (1979) 1080–1084.
[41] N. Orlovskaya, H. Peterlik, M. Marczewski, K. Kromp, J. Mater. Sci. 32 (1997) 1903–1907.
[42] N. Orlovskaya, H. Peterlik, W. Steinkellner, K. Kromp, J. Mater. Sci. 35 (2000) 699–705.
[43] N. Orlovskaya, H. Peterlik, W. Steinkellner, K. Kromp, J. Mater. Sci. 35 (2000) 707–711.
[44] M. Radovic, E. Lara-Curzio, L. Reiser, Mater. Sci. Eng. 368 (2004) 56–70.
[45] A. Atkinson, A. Selcuk, Acta Mater. 47 (1999) 867–874.
[46] A. Atkinson, A. Selcuk, Solid State Ionics 134 (2000) 59–66.
[47] S. Pathak, D. Steinmetz, J. Kuebler, A. Payzant, N. Orlovskaya, Ceram. Int. 35 (3) (2009) 1235–1241.
[48] M. Hirano, S. Watanabe, E. Kato, Y. Mizutani, M. Kawai, Y. Nakamura, Solid State Ionics 111 (1998) 161–169.